J Nanopart Res (2015) 17:239
DOI 10.1007/s11051-015-3048-8

RESEARCH PAPER

Effect of reduction enhancer on a radiolytic synthesis of carbon-supported Pt–Cu nanoparticles and their structural and electrochemical properties

Junichiro Kugai · Chihiro Kubota · Tomohisa Okazaki · Satoshi Seino · Takashi Nakagawa · Hiroaki Nitani · Takao A. Yamamoto

Received: 11 December 2014 / Accepted: 21 May 2015 / Published online: 2 June 2015

Abstract In order to clarify the effect of reduction enhancer on the nanoparticle formation process and their structural and catalytic properties, carbon-supported Pt–Cu nanoparticles were synthesized by electron beam irradiation on an aqueous precursor solution in the presence/absence of reduction enhancer. In the absence of reduction enhancer, tetravalent platinum oxide particles of approximately 1 nm in diameter were formed on carbon support with copper barely precipitated, while in the presence of 2-propanol or ethylene glycol or glucose both platinum and copper precipitated as few-nanometer-sized alloy particles together with copper oxides. It was suggested that the metal nuclei produced upon electron beam irradiation do not have enough lifetime without reduction enhancer due to fast oxidation of the nuclei by oxidizing radicals, while the reduction enhancer scavenges these oxidizing radicals preventing oxidation of metallic clusters and prolonging their lifetime. Ethylene glycol gave smaller and better alloyed particles with less copper oxides compared to 2-propanol since the carbonyl compounds derived from oxidation of ethylene glycol protect metallic clusters from oxidation further prolonging their lifetime. In the electrochemical measurements, the methanol oxidation activities of Pt–Cu/C catalysts were well explained by their structural characteristics.

Keywords Electron beam irradiation · Radiolytic process · Pt–Cu · Nanoparticles · Reduction enhancer · Methanol oxidation

J. Kugai · C. Kubota · T. Okazaki · S. Seino · T. Nakagawa · T. A. Yamamoto
Graduate School of Engineering, Osaka University, 2-1 Yamadaoka, Suita, Osaka 565-0871, Japan

Present Address:
J. Kugai (✉)
Department of Applied Chemistry, Kobe City College of Technology, 8-3 Gakuen-higashimachi, Nishi-ku, Kobe, Hyogo 651-2194, Japan
e-mail: jkugai@kobe-kosen.ac.jp

H. Nitani
Institute of Materials Structure Science (IMSS), High Energy Accelerator Research Organization, 1-1 Oho, Tsukuba, Ibaraki 305-0801, Japan

Introduction

Synthesis of structure- and size-controlled monometallic and bimetallic nanoparticles is of researchers' interest since they play critical roles in catalysis in the energy conversion processes (Heggen et al. 2012). For the catalyst in polymer electrolyte fuel cells, the noble metals are the active components and a great effort has been made for reducing material cost by increasing mass activity of catalyst through optimizing the particle size and shape (Corradini et al. 2012; Dixon et al. 2013; Lei et al. 2014; Takasu et al. 2000) and through modifying the electronic structure of a noble component with a second component (Hsieh and Lin 2009;

Koh and Strasser 2007; Stamenkovic et al. 2006a). In view of size and shape control, liquid-phase processes have been widely used for catalyst synthesis. The polyol method is one of the common and simple processes, but the process requires use of a large quantity of alcoholic solvent, and therefore recycling or treatment of waste solvent is necessary. In some cases, a polymer stabilizer employed for controlling particle size blocks active surface of the catalyst and has to be removed by a chemical or heat treatment before catalytic reaction (Kuo et al. 2006; Roy and Bhattacharya 2013). Meanwhile, a radiation-induced reduction method is a simple one-pot process for the synthesis of nanoparticles, which can be carried out in aqueous media without any polymer stabilizer or post-treatment (Belloni 2006; Belloni et al. 1998). Our laboratory has synthesized various Pt-based bimetallic nanoparticles and demonstrated that irradiating a high-energy electron beam on a metal precursor solution with support powder dispersed in it yields supported fine nanoparticles only in several seconds of time scale (Seino et al. 2008; Yamamoto et al. 2010, 2011). The solvent water is radiochemically decomposed to give hydrated electrons which in turn reduce metal ions to metal nanoparticles:

$$H_2O \rightarrow e^-(aq),\ H_3O^+,\ H\cdot,\ OH\cdot \qquad \text{(Reaction 1)}$$

$$M^+ + e^-(aq) \rightarrow M^0 \qquad \text{(Reaction 2)}$$

The conditions for the radiolytic synthesis have a large impact on the structure of resulting particles. In the synthesis of carbon-supported Pt–Ru, addition of bicarboxylates such as tartaric acid and citric acid to the precursor solution enhanced alloying of Pt and Ru (Kageyama et al. 2011). It was found that the presence of bicarboxylates decreases the reduction potential of platinum, which makes reduction of platinum ions slower and gives more chances for ruthenium to bind with platinum (Daimon et al. 2008). In a polyol method, citric acid has been employed as a stabilizer for small colloidal particles (Guo et al. 2005). During the reflux of polyol, citric acid adsorbs on the metal surface to suppress particle growth (Ozkar and Finke 2002). Addition of phosphorous was shown to reduce particle size significantly in the radiolytic synthesis (Daimon and Kurobe 2006). Phosphorous is known to disconnect crystallographic continuity of metal, as it was demonstrated in electroless plating of nickel on a substrate (Daimon et al. 1989). The particle size was even smaller in the presence of copper in nanoparticles since both phosphorous and copper decrease periodicity of platinum lattice structure. Alcohol is added as a reduction enhancer in a radiolytic synthesis. The alcohol molecules scavenge oxidizing radicals such as hydroxyl radicals to give alcohol radicals which contribute to the reduction of metal ions (Barta et al. 2010; Belloni and Mostafavi 2001):

$$OH\cdot + CH_3CH(OH)CH_3 \rightarrow H_2O + CH_3C\cdot(OH)CH_3 \qquad \text{(Reaction 3)}$$

$$M^+ + CH_3C\cdot(OH)CH_3 \rightarrow M^0 + CH_3COCH_3 + H^+ \qquad \text{(Reaction 4)}$$

However, the effect of the type of alcohol has little been investigated for supported bimetallic systems.

In the present study, carbon-supported Pt and Pt–Cu nanoparticles were synthesized in the absence and presence of various reduction enhancers in order to investigate its effect on the nanoparticle formation process. Three alcohols (2-propanol, ethylene glycol, and glucose) were chosen for the Pt and Pt–Cu syntheses in order to compare the effects of monohydric and polyhydric alcohols to enhance the reduction of metal ions and to stabilize metal nuclei or clusters in the particle formation process. The obtained catalyst was characterized by inductively coupled plasma atomic emission spectroscopy, X-ray diffraction, and transmission electron microscope. Electrochemical properties were evaluated by the cyclic voltammetry (CV) and chronoamperometry in acidic solution containing methanol.

Experimental

The precursor solution was prepared using H_2PtCl_6 and $CuSO_4$ as metal salts and water as a solvent. Support powder (carbon black: Vulcan XC-72R from Cabot: $\sim$250 m^2/g of surface area and $\sim$30 nm of particle size) was dispersed in the precursor solution. Either of 2-propanol, ethylene glycol, or glucose was added as a reduction enhancer and compared with the sample without it. Argon gas was bubbled through the solution to remove dissolved oxygen. The solution was sealed in a glass vial and then irradiated with 4.8 MeV of electron beam for 6–7 s (3 kGy/s of dose rate at the surface of the solution) at a commercial facility for sterilization of medical supplies (Japan Electron Beam Irradiation Service Co. at Osaka,

Japan). The product, nanoparticles of platinum and copper supported on carbon, was separated by filtration, dried at 80 °C overnight, and served for chemical and structural analyses. The synthesis conditions are summarized in Table 1.

The composition of catalyst was analyzed by an inductively coupled plasma atomic emission spectroscopy (ICP-AES, ICPE-9000, Shimadzu). The crystal structure of Pt–Cu nanoparticle was analyzed by X-ray diffraction (XRD, RINT2100-Ultima with Cu-$K\alpha$ radiation, Rigaku). The lattice parameter of nanoparticle was estimated from the diffraction angle using the Bragg's equation:

$$d = \Lambda/2\ \sin\theta, \quad (1)$$

where d is the lattice spacing, Λ is the wavelength of incident X-ray (1.5418 Å for Cu-$K\alpha$), and θ is the Bragg angle. The lattice parameter was further converted to the composition of Pt–Cu alloy assuming a linear relationship of lattice constant to copper content in the alloy [Vegard's law (Vegard 1921)]. The average particle size was estimated from the line broadening using the Scherrer's equation:

$$\tau = K\Lambda/(\beta\cos\theta), \quad (2)$$

where τ is the crystallite size, K is the shape factor (0.85 for spherical crystallites), and β is the line broadening at half the maximum intensity (FWHM). The morphology and size of supported nanoparticles were investigated by transmission electron microscope (TEM, H-8100, Hitachi).

Electrochemical measurements were conducted using a three-electrode cell and a potentiostat (Versastat 4-200, Princeton Applied Research). A gold wire and an Ag/AgCl electrode were used as the counter and reference electrodes, respectively. For the working electrode, 15 μL of catalyst ink was applied onto 0.2 cm^2 of a flat surface of glassy carbon (GC) electrode (the catalyst ink was prepared by dispersing 10 mg of catalyst in 5 mL of pure water followed by adding 10 % Nafion ionomer solution by 0.2 vol%). CV was performed in 0.5 M H_2SO_4 aqueous media in a potential range from 0.06 to 1.23 V versus RHE at a scan rate of 0.1 V/s. The electrochemical surface area (ECSA) was calculated by integrating the charge involved in hydrogen monolayer adsorption in the fiftieth cycle of CV assuming that 2.10 C of charge is involved in hydrogen adsorption on 1 m^2 of Pt surface. After 50 cycles, methanol was added to the aqueous media to achieve 0.185 M of methanol concentration, and CV was performed in the same sweep range and sweep rate. Chronoamperometry was subsequently performed at 0.7 V versus RHE for 20 min. All the measurements were performed in N_2 atmosphere at 30 °C.

Results and discussion

Effect of reduction enhancers

The compositions of Pt–Cu/C, Pt/C, and Cu/C samples synthesized in the presence of various reduction enhancers are summarized in Table 2. Without any

Table 1 Synthesis conditions of carbon-supported Pt, Pt–Cu, and Cu catalysts

Sample ID	H_2PtCl_6 (mM)	$CuSO_4$ (mM)	Carbon (g/L)	Reduction enhancer (M)	Atmosphere
Pt5Cu5(2-Pr)	0.67	0.67	0.92	0.35 (2-Propanol)	Argon or air
Pt5Cu5(EG)				0.30 (Ethylene glycol)	
Pt5Cu5(Glu)				0.10 (Glucose)	
Pt5Cu5(N)				0	
Pt5(2-Pr)	0.67	0	0.92	0.35 (2-Propanol)	Argon or air
Pt5(EG)				0.30 (Ethylene glycol)	
Pt5(N)				0	
Cu9(2-Pr)	0	1.2	0.92	0.35 (2-Propanol)	Argon
Cu9(EG)				0.30 (Ethylene glycol)	
Cu9(N)				0	
Pt1Cu9(2-Pr)	0.13	1.2	0.92	0.35 (2-Propanol)	Argon or air
Pt1Cu9(EG)				0.30 (Ethylene glycol)	

reduction enhancer, Pt and Cu loadings were 7.4 and 0.37 wt%, which correspond to only 60 and 10 % of target Pt and Cu loadings, respectively. For the monometallic cases, Pt loading was 8.4 wt% for Pt/C and Cu loading was 0.07 wt% for Cu/C. Therefore, alcohol has a great impact on the reduction of metal ions in aqueous media, particularly on the reduction of copper. By adding 2-propanol or ethylene glycol or glucose, most of Pt and Cu were reduced and deposited on carbon support. A slightly lower Pt loading than the target value would be an artifact in the ICP-AES measurement that originates from incomplete dissolution of metal species adsorbed on carbon support in aquilegia. A part of platinum could form unsupported colloidal particles and washed away by filtration also. The monometallic copper gave only about 40 % of the target loading, but in the copresence of a small amount of Pt, Cu loading increased significantly (see the copper loading of Pt1Cu9/C sample compared to that of Cu9/C in Table 2), suggesting that copper reduction is also enhanced in the presence of platinum (Kugai et al. 2011).

The XRD patterns of Pt–Cu/C, Pt/C, and Cu/C samples are shown in Fig. 1a and b. The Pt/C had a peak at 39.8° which corresponds to the diffraction from Pt(111) plane, while the Cu/C samples had a peak at 43.2° which corresponds to the diffraction from Cu(111) plane. Pt–Cu/C had a diffraction peak between them, indicating Pt–Cu alloy formation. The lattice parameter estimated by Eq. (1), the alloy composition (Cu/Pt ratio in alloy crystal) estimated with the assumption of Vegard's law, and the average crystallite size estimated by Eq. (2) are summarized in Table 3. The samples made in the absence of reduction enhancer showed much smaller peaks than those made in the presence of it, indicating that the crystal is not well developed. There was no peak observed for Cu9(N), consistent with its low Cu loading (Table 2). The Pt5(N) showed a sharp low-intensity peak and thus it contains a few, but large, crystallites. Pt5Cu5(EG) and Pt5Cu5(Glu) showed smaller crystallite size and higher alloying degree than Pt5Cu5 (2-Pr). Such effects of ethylene glycol and glucose on the structural characters of particles resemble those of bicarboxylate additives (tartrate, citrate, etc.). The bicarboxylate is known to form a platinum complex to decrease the reduction potentials of platinum and to

Table 2 Effect of reduction enhancers on metal loadings of Pt/C, Pt–Cu/C, and Cu/C catalysts

Sample ID	Pt (wt%)	Cu (wt%)	$Cu/Pt_{catalyst}$ ratio
Pt5Cu5(2-Pr)	10.0	3.6	1.1
Pt5Cu5(EG)	9.6	3.3	1.0
Pt5Cu5(Glu)	9.2	3.2	1.1
Pt5Cu5(N)	7.4	0.37	0.15
Pt5(2-Pr)	10.1	–	–
Pt5(EG)	10.7	–	–
Pt5(N)	8.4	–	–
Cu9(2-Pr)	–	3.2	–
Cu9(EG)	–	2.9	–
Cu9(N)	–	0.07	–
Pt1Cu9(2-Pr)	2.1	5.4	8.0
Pt1Cu9(EG)	2.1	3.8	5.7

The aimed compositions were 11.9 wt% Pt and 3.88 wt% Cu (Cu/Pt atomic ratio = 1.0) for Pt5Cu5/C, 12.4 wt% Pt for Pt5/C, 7.65 wt% Cu for Cu9/C, and 2.5 wt% Pt and 7.5 wt% Cu (Cu/Pt atomic ratio = 9.0) for Pt1Cu9/C

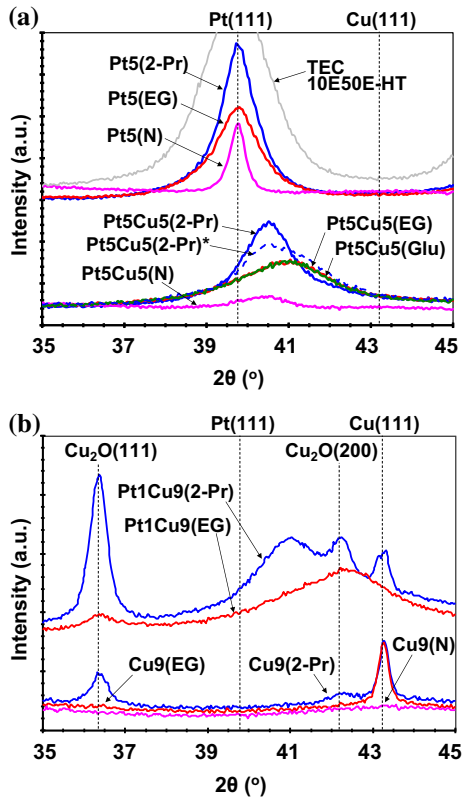

Fig. 1 XRD patterns of Pt/C, Pt–Cu/C, and Cu/C catalysts. **a** Pt5/C and Pt5Cu5/C samples prepared with various reduction enhancers. **b** Pt1Cu9/C and Cu9/C samples prepared with various reduction enhancers

Table 3 Effect of reduction enhancers on average crystallite size, lattice parameter, and alloying degree of Pt–Cu estimated from the broadening and 2θ of Pt(111) diffraction peak

Sample ID	Average crystallite size (nm)	Lattice parameter (Å)	Cu/Pt_{alloy} ratio
Pt5Cu5(2-Pr)	5.5	3.856 ± 0.007	0.28 ± 0.04
Pt5Cu5(2-Pr)[a]	3.4	3.852 ± 0.011	0.30 ± 0.06
Pt5Cu5(EG)	3.1	3.814 ± 0.012	0.55 ± 0.09
Pt5Cu5(Glu)	3.2	3.814 ± 0.011	0.55 ± 0.09
Pt5Cu5(N)	5.7	3.861 ± 0.007	0.26 ± 0.04
Pt5(2-Pr)	8.4	3.925 ± 0.005	0.00 ± 0.01
Pt5(EG)	6.5	3.925 ± 0.005	0.01 ± 0.02
Pt5(N)	19.0	3.926 ± 0.002	0.01 ± 0.02
TEC 10E50E-HT	4.6	3.927 ± 0.008	0.01 ± 0.03
Cu9(2-Pr)	29.1[b]	–	–
Cu9(EG)	27.0[b]	–	–
Pt1Cu9(2-Pr)	3.2	3.813 ± 0.011	0.56 ± 0.09
Pt1Cu9(EG)	2.7	3.692 ± 0.012	2.99 ± 0.73

The error range of peak position was assumed to be ±5 % of FWHM

[a] Prepared with the same precursor as Pt5Cu5(2-Pr) in another lot

[b] Crystallite size estimated from Cu(111) peak at $2\theta = 43.2°$

promote their alloying (Daimon et al. 2008; Kageyama et al. 2011). It also has a function of a stabilizer for nanoparticles (Xu et al. 2006). The similarity in the effects indicates that not only ethylene glycol or glucose works as a scavenger for oxidizing radicals, but its oxidized product, glycolaldehyde (Soroushian et al. 2005) or glycolate formed through the reaction equations below, functions as a chelating agent for platinum ions and as a stabilizer for metal nuclei, slowing platinum reduction and prolonging the lifetime of metal nuclei producing small well-alloyed nanoparticles. Such multi-functions of ethylene glycol were also reported for a polyol process where ethylene glycol is a reductant and its oxidation product, glycolate, is a stabilizer for small nanoparticles (Bock et al. 2004). It is conceivable that the ability of the functional group to coordinate to metal surface is strongly influenced by the other functional group at the β-position through electronic and geometric interactions.

$$OH\cdot + HOCH_2CH_2OH \rightarrow H_2O + HOCH_2CH\cdot OH \quad \text{(Reaction 5)}$$

$$M^+ + HOCH_2CH\cdot OH \rightarrow M^0 + HOCH_2CHO + H^+ \quad \text{(Reaction 6)}$$

$$2\ M^+ + HOCH_2CHO + H_2O \rightarrow 2\ M^0 + HOCH_2COOH + 2H^+ \quad \text{(Reaction 7)}$$

The dielectric property of ethylene glycol would also contribute to stabilizing small particles (Bock et al. 2004). For the Cu-rich samples (Pt1Cu9/C and Cu9/C), ethylene glycol yielded less copper oxide phase than 2-propanol (Fig. 1b). The XRD pattern of Pt1Cu9(EG) showed little crystalline Cu_2O (36.4°, 42.2°) or monometallic Cu (43.2°), instead much higher extent of alloying compared to that of Pt1Cu9(2-Pr). The XRD peaks at 36.4° and 42.2° for Pt1Cu9(2-Pr) and Cu9(2-Pr) are of (111) and (200) crystal planes of Cu_2O, respectively, which suggests that the excess copper isolated from platinum is alternatively stabilized by the formation of oxide and crystallization of it. The results corroborate that not only ethylene glycol slows platinum reduction to incorporate more copper in the particles, but its oxidized form (glycolaldehyde or glycolate) protects metallic or alloyed clusters from fast crystal growth (for Pt-rich conditions) and oxidation (for Cu-rich conditions) increasing their lifetime before they deposit on the carbon support.

In Fig. 2, Pt L_3-edge XANES spectra of Pt/C and Pt–Cu/C samples are presented. The white line of the

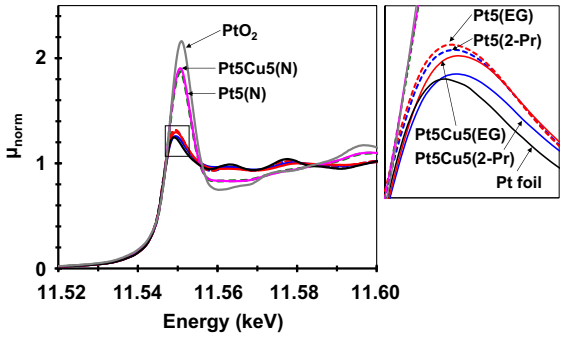

Fig. 2 Pt L_3-edge XANES of Pt/C and Pt–Cu/C catalysts. The *inset* is the magnification of the area marked by the *square*

spectra was fitted to a linear combination of Pt metal and PtO_2 spectra, and the results are summarized in Table 4. It is obvious that platinum is mainly tetravalent oxides without reduction enhancer. Therefore, the crystalline Pt identified in the diffraction pattern in Fig. 1a is a minor product, and the platinum oxide invisible in XRD is a major product for the samples without reduction enhancer. The platinum precursor is probably reduced once, but the lifetime of the reduced species is too short without reduction enhancer, resulting in the oxidation of platinum to oxide and copper to ionic state. With reduction enhancers, on the other hand, platinum was almost metallic. From the magnification of the white line of spectra, Pt in Pt–Cu/C is slightly more metallic than Pt in Pt/C. This can be explained by a shift of platinum d-band states toward higher binding energy by alloying, resulting in higher electron density on platinum (Anniyev et al. 2010). Slightly oxidic feature with ethylene glycol compared to 2-propanol could be due to size effect where the capping oxygen atoms on small particles raise white line intensity of XANES spectra.

In Fig. 3, Cu *K*-edge XANES spectra of Pt–Cu/C and Cu/C samples are presented. In consistent with Pt L_3-edge spectra, Cu in Pt–Cu was more oxidic than Cu in Cu/C. Thus, in Pt–Cu alloy, electron is transferred from Cu to Pt. Such electron transfer was also identified in XPS study (Peng et al. 2014; Wang et al. 2011). The Cu in Cu9(EG) was more metallic than Cu9(2-Pr) in good agreement with the XRD results. It was confirmed that ethylene glycol protects copper from oxidation.

The EXAFS spectra were fitted to a theoretical equation, and the fitting parameters are summarized in Table 5. Typical scattering components of Pt L_3-edge fit are also shown in Fig. 4. The fits of Pt L_3-edge spectra showed the presence of both Pt–Pt and Pt–Cu bonds in Pt–Cu/C samples. The ratio of Pt–Cu coordination number to Pt–Pt was somewhat larger for Pt5Cu5(EG) than Pt5Cu5(2-Pr) in good agreement with the XRD data. The average bond distances were between 3.77 Å (Pt–Pt distance of pure Pt) and 2.55 Å (Cu–Cu distance of pure Cu). The Pt–Pt and Pt–Cu bond distances were closer to each other for Pt5Cu5(EG) than those for Pt5Cu5(2-Pr), indicating that the two components in the former are better mixed (alloyed) with each other. The coordination numbers for the two Pt/C samples were close to each other regardless of some difference in crystallite size estimated from the broadening of diffraction peak possibly because the most of Pt–Pt scatter comes from the bulk of Pt crystal for the large crystallites. The fits of Cu *K*-edge spectra also showed that both the elements are present in the neighbor of Cu atoms. The coordination number of Cu–Cu was <1, while that of Cu–Pt was 3–4, suggesting that metallic Cu atoms are surrounded mainly by Pt atoms. The larger Cu–Pt coordination number and longer Cu–Pt bond distance for the Pt5Cu5(EG) sample than Pt5Cu5(2-Pr) again show better alloying. The Cu–O bonds are of capping oxygen and of CuO_x phase. The fits of Cu *K*-edge spectra of Cu/C samples revealed the presence of metallic Cu with less CuO_x compared to those of Pt–Cu/C. A larger coordination number for Cu9(EG) than Cu9(2-Pr) supports that carbonyl compounds (glycolaldehyde and glycolate) derived from ethylene glycol protect metallic copper particles from oxidation.

In Fig. 5, transmission electron microscope images of Pt–Cu/C samples are compared. The samples prepared with reduction enhancers had particles with 2–4 nm diameter. The particle size is in the similar range to the crystallite size estimated from the line broadening of XRD. Thus, each particle consists of a single crystallite. Some aggregations were observed though they are not shown in the figure. The smaller particle size (observed in TEM) than the crystallite size (estimated from XRD) for the Pt5Cu5(2-Pr) sample indicates that there are larger particles (crystallites) in the aggregates in which each particle size cannot be measured. The sample without reduction enhancer had much smaller particles. The particle with 1 nm diameter consists of only a few dozens of atoms at the maximum. They were highly dispersed and fewer aggregations were observed. This confirms that

Table 4 Linear combination fittings of XANES spectra of Pt/C, Pt–Cu/C, and Cu/C catalysts

Sample ID	Pt (%)	PtO_2 (%)	Cu (%)	Cu_2O (%)	CuO, $CuSO_4$ (%)
Pt5Cu5(2-Pr)	95	5	25	13	62
Pt5Cu5(EG)	91	9	24	21	55
Pt5Cu5(N)	29	71	9	0	91
Pt5(2-Pr)	92	8	–	–	–
Pt5(EG)	91	9	–	–	–
Pt5(N)	32	68	–	–	–
Cu9(2-Pr)	–	–	44	33	23
Cu9(EG)	–	–	71	0	29

Pt L_3-edge spectra were fitted to those of Pt metal and PtO_2. Cu *K*-edge spectra were fitted to those of Cu metal, Cu_2O, CuO, and $CuSO_4$

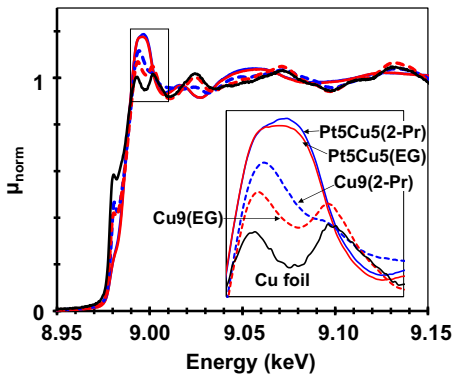

Fig. 3 Cu *K*-edge XANES of Pt–Cu/C and Cu/C catalysts. The *inset* is the magnification of the area marked by the *square*

the lifetime of the platinum reduced by an electron beam irradiation is too short in the absence of a reduction enhancer and quickly oxidized to PtO_2.

Effect of dissolved oxygen

In order to examine the impact of dissolved oxygen on metal loadings and oxide formation, the samples were synthesized under the same conditions except that the precursor solution was air-bubbled before electron beam irradiation. In Table 6, metal loadings of samples prepared from air-exposed precursors were compared with those prepared from argon-bubbled solutions. The products obtained from air-exposed solutions in general have less copper loading and less copper in alloy than those obtained from argon-bubbled ones. By changing the atmosphere from argon to air, platinum loading was not much influenced, but the copper loading was lowered, particularly for low-Pt samples (Pt1Cu9/C samples). Therefore, dissolved oxygen mainly inhibits copper reduction. Reducing radicals are scavenged by oxygen (Barr and Allen 1959), and the reduced copper is easily reoxidized by O_2.

Table 5 Fits of Pt L_3-edge and Cu *K*-edge EXAFS spectra of Pt/C, Pt–Cu/C, and Cu/C catalysts

Sample ID	*R* factor	Scatter	*R*(Å)	*N*
Pt5Cu5(2-Pr)				
Pt-L_3	0.0041	Pt–Pt	2.73	5.4
		Pt–Cu	2.65	2.1
		Pt–O	1.96	0.90
Cu-*K*	0.013	Cu–Cu	2.57	0.49
		Cu–Pt	2.65	3.4
		Cu–O	1.95	2.2
Pt5Cu5(EG)				
Pt-L_3	0.0051	Pt–Pt	2.71	4.5
		Pt–Cu	2.67	2.4
		Pt–O	2.01	0.89
Cu-*K*	0.012	Cu–Cu	2.58	0.68
		Cu–Pt	2.67	3.9
		Cu–O	1.93	1.8
Pt5(2-Pr)				
Pt-L_3	0.0031	Pt–Pt	2.76	7.4
		Pt–O	1.94	0.79
Pt5(EG)				
Pt-L_3	0.0034	Pt–Pt	2.76	7.3
		Pt–O	1.98	0.76
Cu9(2-Pr)				
Cu-*K*	0.051	Cu–Cu	2.54	3.8
		Cu–O	1.89	0.93
Cu9(EG)				
Cu-*K*	0.008	Cu–Cu	2.54	6.6
		Cu–O	1.91	0.54

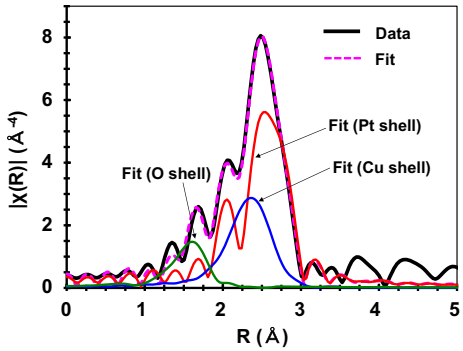

Fig. 4 Typical fitting of Fourier transform of Pt L_3-edge EXAFS [Pt5Cu5(EG) sample]

$$e^- + O_2 \rightarrow O_2^- \quad \text{(Reaction 8)}$$

$$H\cdot + O_2 \rightarrow HO_2\cdot \quad \text{(Reaction 9)}$$

In Fig. 6, comparisons of XRD patterns were made for the samples prepared in argon and air atmospheres. The lattice parameter, the alloy composition, and the average crystallite size estimated from the Pt(111) peak are summarized in Table 7. For Pt5Cu5/C, oxygen did not much impact the alloying. However, for Pt1Cu9/C, the diffraction peak of Pt(111) plane shifted to lower angle with air exposure, i.e., alloying was inhibited by oxygen. Thus, higher concentration of Pt source facilitates copper incorporation into Pt against copper oxidation. Fewer platinum allows reoxidation of copper species to ionic state by oxygen which were otherwise to be incorporated into Pt crystal for Pt1Cu9(EG) or stabilized as monometallic Cu, crystalline Cu_2O, and Pt–Cu alloy for Pt1Cu9 (2-Pr). Copper is stabilized only by coalescing with platinum in the presence of oxygen.

Electrochemical measurements

Figure 7 shows the cyclic voltammograms of Pt–Cu/C and Pt/C samples coated on a GC electrode in N_2-purged acidic media. All showed typical butterfly-type voltammograms. Therefore, the surface of Pt–Cu nanoparticles was dealloyed and composed of platinum shell. A commercial Pt/C catalyst (TEC 10E50E-HT) showed largest current over the entire potential range due to its high Pt loading (50.8 %). The cathodic and anodic current peaks in the potential range of 0.06–0.4 V are of adsorption and desorption of hydrogen on Pt surface, respectively. Three hydrogen desorption peaks at around 0.13, 0.18, and 0.26 V are considered as hydrogen desorption from specific facets. These could be assigned to hydrogen desorption from (111) crystal plane, edge sites, and (100) crystal plane of platinum based on literature (Kinoshita et al. 1973; Kinoshita and Stonehart 1975; Rao et al. 2011; Ross Jr 1979). The assignment of the middle peak to edge sites is consistent with the fact that Pt5Cu5(N) is composed of small particles. The ECSA estimated from the hydrogen adsorption peak was in the range of 20–70 m^2/g Pt (See Fig. 8). The order of ECSA among the Pt–Cu catalysts was Pt5Cu5(N) > Pt5Cu5(EG) > Pt5Cu5(2-Pr), which seems to reflect the particle size. Monometallic Pt(EG) had somewhat higher ECSA than Pt5Cu5(2-Pr) regardless of its larger particle size possibly owing to a stronger hydrogen adsorption (Stamenkovic et al. 2006b). Pt5Cu5(N) showed the largest ECSA because the catalyst consists of Pt particles of 1 nm in size. It is noted that Pt5Cu5(N) showed a large cathodic current in the first cycle of voltammetry. From the difference of the cathodic currents of the first cycle and the fiftieth cycle, about a half of Pt^{4+} species were reduced to Pt^0 in the first cycle and more in the subsequent cycles. Thus, at least the surface of subnanometer tetravalent platinum oxide particles in Pt5Cu5(N) were reduced to metallic state in the N_2-purged acid solution under the potential scan. The anodic current above 0.8 V and cathodic current at 0.6–0.8 V are of oxygen adsorption and desorption, respectively. The order of peak intensity was similar to the hydrogen adsorption/desorption peaks. A long tail of cathodic peak for Pt5Cu5(N) is typical of strong retention of oxygen on the surface of small particles (Jayasayee et al. 2012).

Figure 9 shows the results of cyclic voltammetry performed in a methanol–added acidic media. The current was normalized by actual platinum surface area. Although Pt–Cu has been reported as a highly active catalyst for oxygen reduction reaction (Stamenkovic et al. 2006a; Strasser et al. 2010), recent studies have shown that the catalyst is also effective for methanol oxidation reaction (Ferrin and Mavrikakis 2009; Papadimitriou et al. 2010). The similar enhancement mechanism has been proposed for both reactions based on the d-band center theory, i.e., Pt–Pt bond distance is shorter in the presence of copper in the core of the particles, which shifts d-band center of surface platinum downwards and weakens the

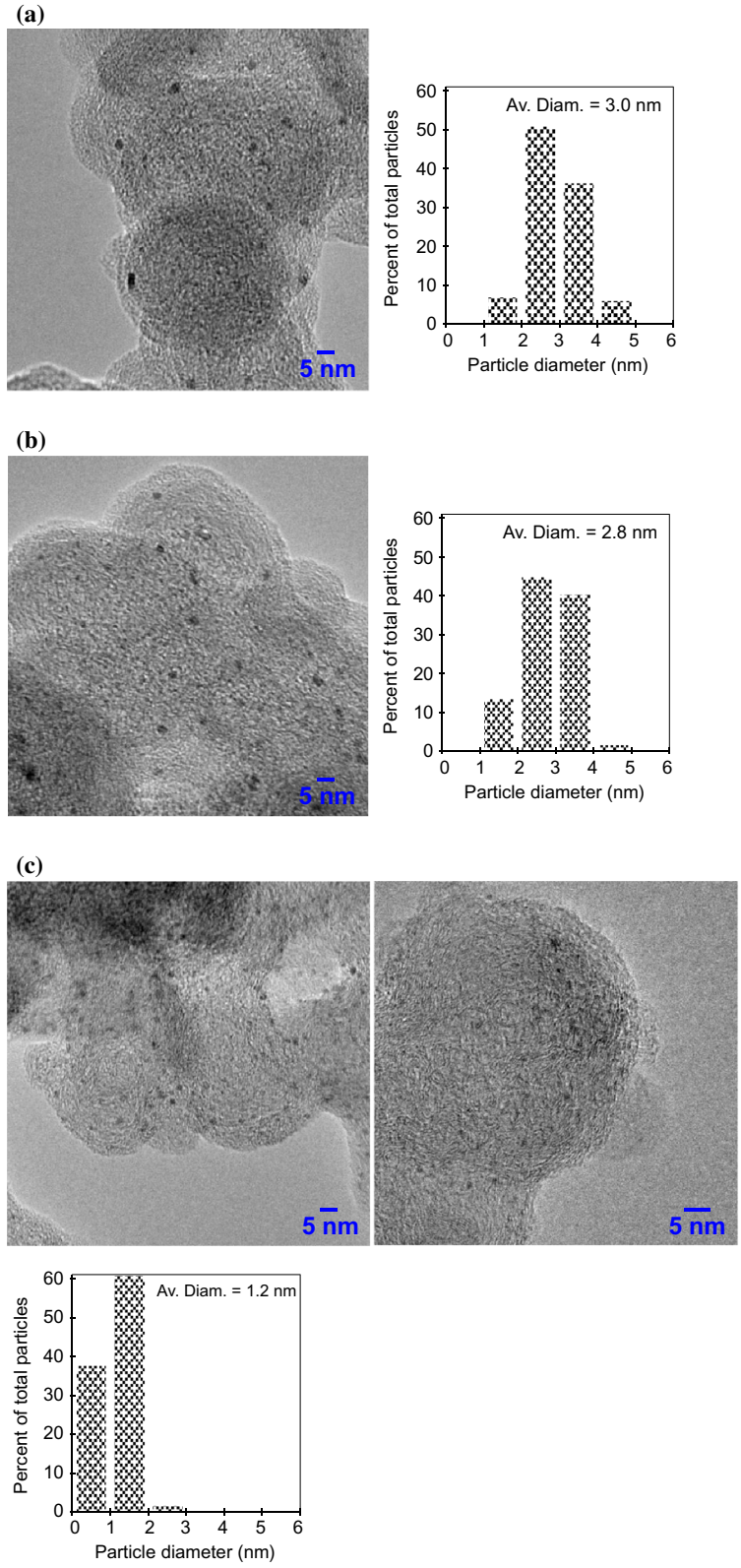

Fig. 5 TEM image and particle size distribution of Pt–Cu/C catalysts prepared with various reduction enhancers: **a** Pt5Cu5(2-Pr); **b** Pt5Cu5(EG); and **c**, **d** Pt5Cu5(N)

Table 6 Effect of dissolved oxygen on metal loadings of Pt–Cu/C catalysts

Sample ID	Pt (wt%)	Cu (wt%)	$Cu/Pt_{catalyst}$ ratio
Pt1Cu9(2-Pr)	2.1	5.4	8.0
Pt1Cu9(2-Pr,air)	2.2	2.0	2.8
Pt1Cu9(EG)	2.1	3.8	5.7
Pt1Cu9(EG,air)	2.2	0.74	1.0
Pt5Cu5(2-Pr)	11.3	3.5	0.95
Pt5Cu5(2-Pr,air)	12.2	3.3	0.84
Pt5(2-Pr)	12.3	–	–
Pt5(2-Pr,air)	11.6	–	–

The aimed compositions were same as samples in Table 2

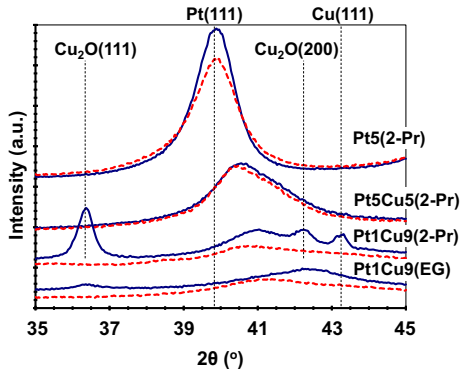

Fig. 6 XRD patterns of Pt–Cu/C catalysts prepared in argon and air atmospheres. *Solid line* argon-bubbled, *dotted lines* air-bubbled

interaction with adsorbates. For all the samples tested, a peak of oxidation current was observed at around 0.8–0.9 V during a positive sweep and at 0.6–0.7 V during a negative sweep. The current in the positive sweep is methanol oxidation to CO_2 and/or intermediates, while the current in the negative sweep is the

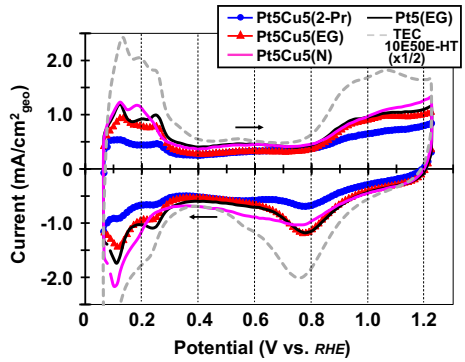

Fig. 7 Cyclic voltammograms of Pt/C and Pt–Cu/C catalysts in an N_2-purged 0.5 M H_2SO_4 aqueous solution. The electrode was prepared by applying catalyst ink (about 30 μg of catalyst) on 0.2 cm^2 flat surface of glassy carbon electrode. The voltammograms are of 50th cycle. Potential range: 0.06–1.23 V (vs. *RHE*), sweep rate: 0.1 V/s, and temperature: 30 °C

oxidation of intermediates to CO_2 according to literature (Hsieh and Lin 2009). The peak current in the positive sweep was in the order of Pt5Cu5 (2-Pr) > Pt5Cu5(EG) > Pt5(EG) ~ TEC 10E50E-HT > Pt5Cu5(N). The higher oxidation current for Pt5Cu5(2-Pr) and Pt5Cu5(EG) than monometallic catalysts indicates a positive effect of copper present in the core of the particles. The lowest activity of Pt5Cu5(N) would be due to a strong adsorption of CO on the surface of small Pt particles (Takasu et al. 2000; Yahikozawa et al. 1991) and a low dehydrogenation activity of methanol on platinum (Bergamaski et al. 2006). The ratio of peak currents in positive and negative sweeps (I_p and I_n) is an indicator of resistance to CO poisoning (Chen et al. 2007; Hsieh and Lin 2009) (Table 8). Commercial TEC 10E50E-HT and Pt5(EG) showed relatively low I_p to I_n, which indicates that the monometallic platinum catalysts tend to accumulate partially oxidized species on the

Table 7 Effect of dissolved oxygen on crystallite size, lattice parameter, and alloying of Pt–Cu estimated by Pt(111) diffraction peaks

Sample ID	Average crystallite size (nm)	Lattice parameter (Å)	Cu/Pt_{alloy} ratio
Pt1Cu9(2-Pr)	3.2	3.813 ± 0.011	0.56 ± 0.09
Pt1Cu9(2-Pr,air)	2.4	3.869 ± 0.016	0.21 ± 0.08
Pt1Cu9(EG)	2.8	3.692 ± 0.012	2.99 ± 0.73
Pt1Cu9(EG,air)	2.2	3.790 ± 0.017	0.76 ± 0.18
Pt5Cu5(2-Pr)	3.7	3.851 ± 0.010	0.31 ± 0.06
Pt5Cu5(2-Pr,air)	3.5	3.868 ± 0.011	0.22 ± 0.05
Pt5(2-Pr)	6.3	3.916 ± 0.006	–
Pt5(2-Pr,air)	5.7	3.916 ± 0.007	–

The error range of peak position was assumed to be ±5 % of FWHM

surface. Thus, copper addition suppresses poisoning of catalyst surface by the intermediates. The result of chronoamperometry is shown in Fig. 10. The initial drop of methanol oxidation current is due to a double-layer formation (Bai et al. 2009; Xu et al. 2011). The subsequent decrease of current is from the accumulation of intermediates on the catalyst surface. Consistent with the CV results, Pt5Cu5(2-Pr) and Pt5Cu5(EG) catalysts were more active than the monometallic catalysts. The better performance for Pt5Cu5(2-Pr) than Pt5Cu5(EG) would be explained by the difference in surface structure. Since Pt5Cu5(EG) has higher copper content in the alloy particles, the copper could leach out from the subsurface layer and the Pt surface after the repetitive potential sweeps is roughened. Meanwhile, Pt5Cu5(2-Pr) with lower copper content could keep copper in the subsurface and create more smooth Pt thin layer on the surface. The latter would compress the Pt–Pt bond distance more effectively, down-shifting d-band center of surface platinum and weakening Pt–CO bonding. Similar comparison of surface structure was made

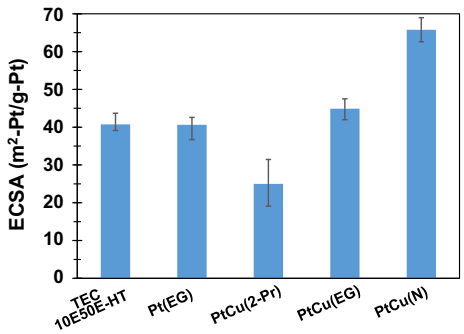

Fig. 8 Electrochemical surface area (ECSA) of Pt/C and Pt–Cu/C catalysts. The *error bar* shows the ECSA range measured for 3–5 times of electrode preparations

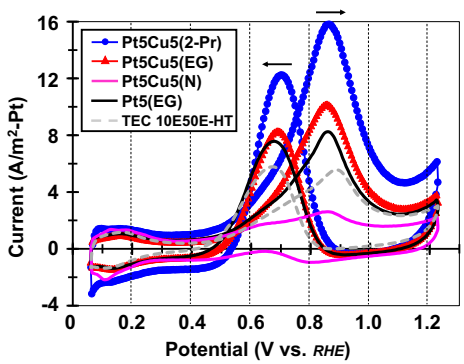

Fig. 9 Specific methanol oxidation current on Pt/C and Pt–Cu/C catalysts in an N_2-purged 0.185 M CH_3OH + 0.5 M H_2SO_4 aqueous solution. Methanol was added by 0.185 M to the 0.5 M H_2SO_4 (aq) electrolyte after the 50 cycles of cyclic voltammetry in the 0.5 M H_2SO_4 solution (Fig. 7). The voltammograms are of 50th cycle. Potential range: 0.06–1.23 V (vs. *RHE*), sweep rate: 0.1 V/s, and temperature: 30 °C

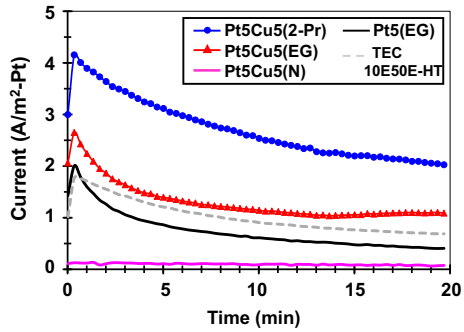

Fig. 10 Specific current–time curves of Pt/C and Pt–Cu/C catalysts in an N_2-purged 0.185 M CH_3OH + 0.5 M H_2SO_4 aqueous solution at 0.7 V. The measurement was conducted after the cyclic voltammetry in the CH_3OH + H_2SO_4 solution (Fig. 9)

Table 8 Electrochemical surface area (ECSA), mass activity, and specific activity for methanol oxidation of Pt/C and Pt–Cu/C catalysts

Sample ID	ECSA[a] (m^2/g Pt)	Peak current in the positive scan I_p		Peak current in the negative scan I_n		I_p/I_n
		(A/m^2 Pt)	(A/g Pt)	(A/m^2 Pt)	(A/g Pt)	
Pt5Cu5(2-Pr)	25.0	14.3	273	14.3	273	1.0
Pt5Cu5(EG)	44.9	9.3	392	9.7	406	0.96
Pt5Cu5(N)	65.8	1.9	314	1.1	374	1.74
Pt5(EG)	40.6	7.4	124	8.8	71	0.84
TEC 10E50E-HT	40.7	4.7	189	6.8	271	0.70

[a] Averaged value of 3–5 measurements

for dealloyed Pt–Co and subsequently annealed Pt–Co, the latter of which better performed in oxygen reduction reaction (Stamenkovic et al. 2006b). The results of electrochemical measurements were well explained by structural properties of Pt–Cu particles synthesized using different reduction enhancers. Copper incorporation has positive effect on methanol oxidation. The Pt5Cu5(2-Pr) has low specific surface, but more ideal surface structure for methanol oxidation, while Pt5Cu5(EG) has high specific surface with well-alloyed bulk structure, but this advantage is canceled out by rough surface.

Conclusion

Carbon-supported Pt–Cu nanoparticles were synthesized by an electron beam irradiation method in the presence/absence of a reduction enhancer. Without reduction enhancer, fine tetravalent platinum oxide particles were formed on carbon support and copper was barely precipitated since metal or alloy cluster is immediately oxidized by oxidizing radicals without reduction enhancer. With 2-propanol, ethylene glycol, or glucose, Pt–Cu alloy nanoparticles and some copper oxides were formed on the carbon support. Ethylene glycol gave smaller and more alloyed Pt–Cu particles with less-isolated copper oxides compared to 2-propanol since an oxidation product of ethylene glycol (glycolaldehyde or glycolate) protects metallic or alloyed clusters and prolongs their lifetime before depositing on the carbon support. The structural features of Pt–Cu/C prepared with various reduction enhancers were correlated to the electrochemical properties. The small Pt particles less than a nanometer prepared without reduction enhancer were detrimental to methanol oxidation because of too strong adsorption of intermediates. The few-nanometer Pt–Cu alloy particles were more active than monometallic Pt catalysts with similar size. The Pt–Cu alloy with moderate copper content prepared with 2-propanol was suggested to create a thin platinum layer on Pt–Cu alloy surface after potential cycles in an acidic solution, which effectively tunes electronic structure of platinum to weaken Pt–CO bond.

Acknowledgments The authors thank Mr. K. Ueno (EBIS, Japan) for the provision of beam time for the electron accelerator. The authors thank partial supports from the Ministry of Education, Culture, Sports, Science and Technology of Japan (Grant-in-Aid No. 22241023 and No. 25410201), and Ministry of Economy, Trade and Industry (R&D Project for Regional Innovation No. 22U5009).

References

Anniyev T, Ogasawara H, Ljungberg MP, Wikfeldt KT, MacNaughton JB, Naslund LA, Bergmann U, Koh S, Strasser P, Pettersson LGM, Nilsson A (2010) Complementarity between high-energy photoelectron and L-edge spectroscopy for probing the electronic structure of 5d transition metal catalysts. Phys Chem Chem Phys 12:5694–5700. doi:10.1039/b926414k

Bai L, Zhu H, Thrasher JS, Street SC (2009) Synthesis and electrocatalytic activity of photoreduced platinum nanoparticles in a poly(ethylenimine) matrix. ACS Appl Mater Interfaces 1:2304–2311. doi:10.1021/am900471f

Barr NF, Allen AO (1959) Hydrogen atoms in the radiolysis of water. J Phys Chem 63:928–931. doi:10.1021/j150576a037

Barta J, Pospisil M, Cuba V (2010) Photo- and radiation-induced preparation of nanocrystalline copper and cuprous oxide catalysts. J Radioanal Nucl Chem 286:611–618. doi:10.1007/s10967-010-0748-5

Belloni J (2006) Nucleation, growth and properties of nanoclusters studied by radiation chemistry—application to catalysis. Catal Today 113:141–156. doi:10.1016/j.cattod.2005.11.082

Belloni J, Mostafavi M (2001) Radiation chemistry of nanocolloids and clusters. In: Jonah CD, Rao BSM (eds) Radiation chemistry: present status and future trends, studies in physical and theoretical chemistry, vol 87. Elsevier Science, Amsterdam, pp 411–452

Belloni J, Mostafavi M, Remita H, Marignier JL, Delcourt MO (1998) Radiation-induced synthesis of mono- and multimetallic clusters and nanocolloids. New J Chem 22:1239–1255. doi:10.1039/A801445K

Bergamaski K, Pinheiro ALN, Teixeira-Neto E, Nart FC (2006) Nanoparticle size effects on methanol electrochemical oxidation on carbon supported platinum catalysts. J Phys Chem B 110:19271–19279. doi:10.1021/jp063337h

Bock C, Paquet C, Couillard M, Botton GA, MacDougall BR (2004) Size-selected synthesis of PtRu nano-catalysts: reaction and size control mechanism. J Am Chem Soc 126:8028–8037. doi:10.1021/ja0495819

Chen W, Kim J, Sun S, Chen S (2007) Composition effects of FePt alloy nanoparticles on the electro-oxidation of formic acid. Langmuir 23:11303–11310. doi:10.1021/la7016648

Corradini PG, Pires FI, Paganin VA, Perez J, Antolini E (2012) Effect of the relationship between particle size, inter-particle distance, and metal loading of carbon supported fuel cell catalysts on their catalytic activity. J Nanopart Res 14:1080. doi:10.1007/s11051-012-1080-5

Daimon H, Kurobe Y (2006) Size reduction of PtRu catalyst particle deposited on carbon support by addition of non-metallic elements. Catal Today 111:182–187. doi:10.1016/j.cattod.2005.10.023

Daimon H, Kitakami O, Fujiwara H (1989) A new method for controlling coercivity of iron deposited alumite films.

J Magn Soc Jpn 13:795–800. doi:10.3379/jmsjmag.13.S1_795

Daimon H, Onodera T, Honda Y, Nitani H, Seino S, Nakagawa T, Yamamoto TA (2008) Activity and durability of PtRuP catalysts and their atomic structures. ECS Trans 11:93–100. doi:10.1149/1.2992497

Dixon D, Melke J, Botros M, Rathore J, Ehrenberg H, Roth C (2013) Increase of catalyst utilization in polymer electrolyte membrane fuel cells by shape-selected Pt nanoparticles. Int J Hydrogen Energy 38:13393–13398. doi:10.1016/j.ijhydene.2013.07.110

Ferrin P, Mavrikakis M (2009) Structure sensitivity of methanol electrooxidation on transition metals. J Am Chem Soc 131:14381–14389. doi:10.1021/ja904010u

Guo JW, Zhao TS, Prabhuram J, Wong CW (2005) Preparation and the physical/electrochemical properties of a Pt/C nanocatalyst stabilized by citric acid for polymer electrolyte fuel cells. Electrochim Acta 50:1973–1983. doi:10.1016/j.electacta.2004.09.006

Heggen M, Oezaslan M, Houben L, Strasser P (2012) Formation and analysis of core-shell fine structures in Pt bimetallic nanoparticle fuel cell electrocatalysts. J Phys Chem C 116:19073–19083. doi:10.1021/jp306426a

Hsieh CT, Lin JY (2009) Fabrication of bimetallic Pt-M (M = Fe, Co, and Ni) nanoparticle/carbon nanotube electrocatalysts for direct methanol fuel cells. J Power Sources 188:347–352. doi:10.1016/j.jpowsour.2008.12.031

Jayasayee K, Van Veen JAR, Manivasagam TG, Celebi S, Hensen EJM, de Bruijn FA (2012) Oxygen reduction reaction (ORR) activity and durability of carbon supported PtM (Co, Ni, Cu) alloys: influence of particle size and non-noble metals. Appl Catal B 111:515–526. doi:10.1016/j.apcatb.2011.11.003

Kageyama S, Seino S, Nakagawa T, Nitani H, Ueno K, Daimon H, Yamamoto TA (2011) Formation of PtRu alloy nanoparticle catalyst by radiolytic process assisted by addition of dl-tartaric acid and its enhanced methanol oxidation activity. J Nanopart Res 13:5275–5287. doi:10.1007/s11051-011-0513-x

Kinoshita K, Stonehart P (1975) Role of platinum surface morphology on hydrogen adsorption isotherms-IV. Electrochim Acta 20:101–107. doi:10.1016/0013-4686(75)85050-X

Kinoshita K, Lundquist J, Stonehart P (1973) Hydrogen adsorption on high surface area platinum crystallites. J Catal 31:325–334. doi:10.1016/0021-9517(73)90302-3

Koh S, Strasser P (2007) Electrocatalysis on bimetallic surfaces: modifying catalytic reactivity for oxygen reduction by voltammetric surface dealloying. J Am Chem Soc 129:12624–12625. doi:10.1021/ja0742784

Kugai J, Kitagawa R, Seino S, Nakagawa T, Ohkubo Y, Nitani H, Daimon H, Yamamoto TA (2011) γ-Fe_2O_3-supported Pt-Cu nanoparticles synthesized by radiolytic process for catalytic CO preferential oxidation. Appl Catal A 406:43–50. doi:10.1016/j.apcata.2011.08.006

Kuo PL, Chen WF, Huang HY, Chang IC, Dai SA (2006) Stabilizing effect of pseudo-dendritic polyethylenimine on platinum nanoparticles supported on carbon. J Phys Chem B 110:3071–3077. doi:10.1021/jp055688m

Lei M, Liang C, Huan Q, Miyabayashi K, Miyake M, Yang T (2014) Morphology-controlled growth of Pt nanoparticles taking advantage of smaller molecule and inorganic salt. Acta Mater 63:202–208. doi:10.1016/j.actamat.2013.10.028

Ozkar S, Finke RG (2002) Nanocluster formation and stabilization fundamental studies: ranking commonly employed anionic stabilizers via the development, then application, of five comparative criteria. J Am Chem Soc 124:5796–5810. doi:10.1021/ja012749v

Papadimitriou S et al (2010) Methanol oxidation at Pt-Cu, Pt-Ni, and Pt-Co electrode coatings prepared by a galvanic replacement process. J Phys Chem C 114:5217–5223. doi:10.1021/jp911568g

Peng X, Zhao Y, Chen D, Fan Y, Wang X, Wang W, Tian J (2014) One-pot synthesis of reduced graphene oxide supported $PtCu_y$ catalysts with enhanced electro-catalytic activity for the methanol oxidation reaction. Electrochim Acta 136:292–300. doi:10.1016/j.electacta.2014.05.110

Rao CS, Singh DM, Sekhar R, Rangarajan J (2011) Pt-Co electrocatalyst with varying atomic percentage of transition metal. Int J Hydrogen Energy 36:14805–14814. doi:10.1016/j.ijhydene.2010.12.142

Ross PN Jr (1979) Structure sensitivity in electrocatalytic properties of Pt: II. Oxygen reduction on low index single crystals and the role of steps. J Electrochem Soc 126:78–82. doi:10.1149/1.2128991

Roy PS, Bhattacharya SK (2013) Size-controlled synthesis and characterization of polyvinyl alcohol-coated platinum nanoparticles: role of particle size and capping polymer on the electrocatalytic activity. Catal Sci Technol 3:1314–1323. doi:10.1039/C3CY20686F

Seino S, Kinoshita T, Nakagawa T, Kojima T, Taniguci R, Okuda S, Yamamoto TA (2008) Radiation induced synthesis of gold/iron-oxide composite nanoparticles using high-energy electron beam. J Nanopart Res 10:1071–1076. doi:10.1007/s11051-007-9334-3

Soroushian B, Lampre I, Belloni J, Mostafavi M (2005) Radiolysis of silver ion solutions in ethylene glycol: solvated electron and radical scavenging yields. Radiat Phys Chem 72:111–118. doi:10.1016/j.radphyschem.2004.02.009

Stamenkovic V, Mun BS, Mayrhofer KJJ, Ross PN, Markovic NM, Rossmeisl J, Greeley J, Norskov JK (2006a) Changing the activity of electrocatalysts for oxygen reduction by tuning the surface electronic structure. Angew Chem Int Ed Engl 45:2897–2901. doi:10.1002/anie.200504386

Stamenkovic VR, Mun BS, Mayrhofer KJJ, Ross PN, Markovic NM (2006b) Effect of surface composition on electronic structure, stability, and electrocatalytic properties of Pt-transition metal alloys: Pt-skin versus Pt-skeleton surfaces. J Am Chem Soc 128:8813–8819. doi:10.1021/ja0600476

Strasser P, Koh S, Anniyev T, Greeley J, More K, Yu C, Liu Z, Kaya S, Nordlund D, Ogasawara H, Toney MF, Nilsson A (2010) Lattice-strain control of the activity in dealloyed core-shell fuel cell catalysts. Nat Chem 2:454–460. doi:10.1038/nchem.623

Takasu Y, Iwazaki T, Sugimoto W, Murakami Y (2000) Size effects of platinum particles on the electro-oxidation of methanol in an aqueous solution of $HClO_4$. Electrochem Commun 2:671–674. doi:10.1016/S1388-2481(00)00101-6

Vegard L (1921) The constitution of the mixed crystals and the filling of space of the atoms. Z Phys 5:17–26. doi:10.1007/BF01349680

Wang H, Wang R, Li H, Wang Q, Kang J, Lei Z (2011) Facile synthesis of carbon-supported pseudo-core@shell PdCu@Pt nanoparticles for direct methanol fuel cells. Int J Hydrogen Energy 36:839–848. doi:10.1016/j.ijhydene.2010.09.033

Xu Y, Xie X, Guo J, Wang S, Wang Y, Mathur VK (2006) Effects of annealing treatment and pH on preparation of citrate-stabilized PtRu/C catalyst. J Power Sources 162:132–140. doi:10.1016/j.jpowsour.2006.07.021

Xu C, Liu Y, Wang J, Geng H, Qiu H (2011) Fabrication of nanoporous Cu-Pt(Pd) core/shell structure by galvanic replacement and its application in electrocatalysis. Appl Mater Interfaces 3:4626–4632. doi:10.1021/am201057t

Yahikozawa K, Fujii Y, Matsuda Y, Nishimura K, Takasu Y (1991) Electrocatalytic properties of ultrafine platinum particles for oxidation of methanol and formic acid in aqueous solutions. Electrochim Acta 36:973–978. doi:10.1016/0013-4686(91)85302-N

Yamamoto TA, Nakagawa T, Seino S, Nitani H (2010) Bimetallic nanoparticles of PtM (M = Au, Cu, Ni) supported on iron oxide: radiolytic synthesis and CO oxidation catalysis. Appl Catal A 387:195–202. doi:10.1016/j.apcata.2010.08.020

Yamamoto TA, Kageyama S, Seino S, Nitani H, Nakagawa T, Horioka R, Honda Y, Ueno K, Daimon H (2011) Methanol oxidation catalysis and substructure of PtRu/C bimetallic nanoparticles synthesized by a radiolytic process. Appl Catal A 396:68–75. doi:10.1016/j.apcata.2011.01.037